Received June 2002
Revised October 2002
Accepted November 2002

REGULAR PAPER

Nonlinear model of linear synchronous reluctance motor for real time applications

Gorazd Štumberger, Bojan Štumberger, Drago Dolinar and Oto Težak
Faculty of Electrical Engineering and Computer Science, University of Maribor, Maribor, Slovenia
Kay Hameyer
Katholieke Universiteit Leuven, Leuven-Heverlee, Belgium

Keywords *Finite element analysis, Electric motors, Modelling*

Abstract *The finite element (FE) method calculations are used to improve dynamic behavior of the two-axis linear synchronous reluctance motor (LSRM) model, which is appropriate for the control design, the real time applications and the low speed servo applications. By the FE method, calculated current and position dependent flux linkages, their partial derivatives and motor thrust are approximated by the continuous functions and incorporated into the dynamic LSRM model as a nonlinear iron core model. The agreement between the calculated and the measured flux linkages, their partial derivatives and the motor thrust is very good. The agreement between all trajectories calculated by the improved dynamic LSRM model and measured during the experiment in the case of kinematic control is very good as well.*

1. Introduction

The finite element (FE) method can provide us with a very accurate distribution of magnetic fields and forces in an electric machine. Unfortunately, the FE models of electric machines are too complex to be appropriate for control synthesis and too time-consuming to be appropriate for the real time applications. On the contrary, the two-axis models of electric machines are not time-consuming and compact, therefore they are appropriate for the control design and real time applications. In two-axis models, magnetic saturation, anisotropy, cross coupling effects and position-dependent force pulsation are normally neglected, which means that only the average value of the force and magnetically linear iron core model are available. In the case of kinematic control at very low speeds and in the case of saturated machine where changes of controlled currents are high and fast, this is not sufficient. In these cases, the magnetically nonlinear model of the iron core and position-dependent force pulsation must be considered in the control synthesis and in the real time application.

COMPEL: The International Journal for Computation and Mathematics in Electrical and Electronic Engineering
Vol. 23 No. 1, 2004
pp. 316-327

0332-1649
DOI 10.1108/03321640410507716

The electrical servo drive is a typical electro-magneto-mechanical coupled problem (Ho *et al.*, 2000; Ren and Razek, 1994; Srairi and Féliachi, 1998). Each servomotor can be decomposed into three distinct subsystems: an electric subsystem, a magnetic subsystem, and a mechanical subsystem (Dawson *et al.*, 1998). The model of the electric subsystem can be given by a set of equations describing voltage balances. The model of the mechanical subsystem describes motion. It contains moving masses, a kinematic chain and different kinds of friction. The electric and the mechanical subsystem are coupled through the magnetic subsystem, whose model is normally given by the FE model. The FE model can give us a very accurate distribution of the magnetic fields and forces.

This work deals with the linear synchronous reluctance motor (LSRM) prototype (Hamler *et al.*, 1998). The LSRM almost always operates under transient conditions because the translation range of motion is limited. Its speed and frequency are very low in comparison to rotary synchronous motors (SM). Therefore the iron losses, very important for the high speed SM applications (Kim *et al.*, 1998; Xu *et al.*, 1991), can be neglected. The interaction between the primary slots and the reluctance secondary causes pulsation of the motor thrust, which is position and current dependent. The mechanical subsystem of the LSRM is a low pass filter, therefore the thrust pulsation is filtered out at high speeds. At low speeds, the thrust pulsation cannot be filtered out and it deteriorates the speed trajectory.

The dynamic model of the LSRM presented in this paper is appropriate for the nonlinear control design and real time realization of low speed servo applications:

(1) for the control design only dynamic models with linear independent state variables are appropriate, where the magnetic nonlinearities are given by continuous functions of state variables;

(2) for the low speed servo applications the position and current dependent motor thrust characteristic must be known very well;

(3) only dynamic models which are compact and fast enough to be calculated together with a control algorithm on a digital signal processor (DSP) in the real time are appropriate for the real time realization.

In the work of Ho *et al.* (2000), Ren and Razek (1994), Srairi and Féliachi (1998), different coupling models of an electromagnetic actuator are discussed. Considering the properties of the LSRM prototype and the required properties of the dynamic LSRM model, only the "parameterization coupling model" (Srairi and Féliachi, 1998) is suitable for the LSRM dynamic model. The LSRM model presented in this paper differs from similar models in the following:

(1) the two-axis LSRM model oriented with the axes of the minimal and the maximal reluctivity is used;

(2) the anisotropic iron core model, which differs from the known models (Boldea and Nasar, 1988; Iglesias *et al.*, 1992; Levi, 1999; Tahan and Kamwa, 1995), is given by the current dependent flux linkages and their partial derivatives;

(3) additionally, the current dependent flux linkages and position and current dependent motor thrust are approximated by the continuous functions in the entire operating range.

The procedure for the calculation of the flux linkage and the motor thrust characteristics of the two-axis LSRM model is presented in this paper. The two-axis LSRM model with lumped parameters is modified. The current dependent flux linkages, their partial derivatives and the position and current dependent thrust are introduced. Their characteristics are calculated by the FE method, approximated by the continuous functions, compared with the measured ones and incorporated into the two-axis LSRM model. The obtained LSRM model contains adequately coupled models (parameterization coupling (Srairi and Féliachi, 1998)) of the electric, magnetic and mechanical subsystem, to be appropriate for the control design and real time realization in the low speed servo application. The proposed LSRM model is confirmed through the comparison of simulation and measured results obtained in the case of kinematic control. The presented results show very good agreement between all calculated and measured trajectories. Even the deterioration of the LSRM speed trajectory caused by the thrust pulsation, which is difficult to obtain with existing two-axis LSRM models, can be seen.

2. Two-axis LSRM model

The direct axis d and the quadrature axis q of the two-axis LSRM model are defined by axes of the minimal and the maximal magnetic reluctance. The two-axis dynamic LSRM model is given by equations (1) and (2):

$$\begin{bmatrix} u_d \\ u_q \end{bmatrix} = R \begin{bmatrix} i_d \\ i_q \end{bmatrix} + \frac{\mathrm{d}}{\mathrm{d}t} \left\{ \begin{bmatrix} \psi_d \\ \psi_q \end{bmatrix} \right\} + \frac{\pi}{\tau_\mathrm{p}} \frac{\mathrm{d}x}{\mathrm{d}t} \begin{bmatrix} -\psi_q \\ \psi_d \end{bmatrix} \tag{1}$$

$$m \frac{\mathrm{d}^2 x}{\mathrm{d}t^2} = F(i_d, i_q, x) - F_l - b \frac{\mathrm{d}x}{\mathrm{d}t} \tag{2}$$

where u_d, u_q, i_d, i_q and ψ_d, ψ_q are the voltages, currents and flux linkages in the d-q reference frame; R is the primary resistance; τ_p is the primary pole pitch; m and x are the mass and the position of the primary; F is the motor thrust; F_l is the load force and b is the coefficient of viscose friction.

For the control purposes the LSRM thrust is normally calculated by:

$$F = \frac{\pi}{\tau_p}(\psi_d i_q - \psi_q i_d) \tag{3}$$

providing only the average value of the current and position dependent thrust, which is unacceptable for the low speed servo applications.

The time derivatives of the flux linkages in equation (1) can be expressed by:

$$\frac{\mathrm{d}}{\mathrm{d}t}\left\{\begin{bmatrix}\psi_d\\ \psi_q\end{bmatrix}\right\} = \begin{bmatrix}\frac{\partial\psi_d}{\partial i_d} & \frac{\partial\psi_d}{\partial i_q}\\ \frac{\partial\psi_q}{\partial i_d} & \frac{\partial\psi_q}{\partial i_q}\end{bmatrix}\frac{\mathrm{d}}{\mathrm{d}t}\left\{\begin{bmatrix}i_d\\ i_q\end{bmatrix}\right\} + \begin{bmatrix}\frac{\partial\psi_d}{\partial x}\\ \frac{\partial\psi_q}{\partial x}\end{bmatrix}\frac{\mathrm{d}x}{\mathrm{d}t} \tag{4}$$

The magnetic subsystem of the LSRM couples the electric subsystem (1) and the mechanical subsystem (2). The magnetically anisotropic behavior of the LSRM iron core is considered by the current dependent flux linkages $\psi_d(i_d, i_q, x)$ and $\psi_q(i_d, i_q, x)$, their partial derivatives and the current and position dependent thrust $F(i_d, i_q, x)$, which are all determined by the FE method based procedure described in Section 3.

The two-phase dynamic LSRM model given by equations (1), (2) and (4) can be used if the instantaneous values of phase voltages u_a, u_b, u_c, phase currents i_a, i_b, i_c, and phase flux linkages ψ_a, ψ_b, and ψ_c of the tested LSRM fulfill the following conditions: $u_a + u_b + u_c = 0$, $i_a + i_b + i_c = 0$ and $\psi_a + \psi_b + \psi_c = 0$.

3. FE calculation

The primary of the LSRM has a three-phase winding with geometric symmetry per phase, used to create the traveling field on the primary whose poles are asymmetric. The primary slots are not skewed. The last five slots on the right and left side of the primary shown in Figure 2 are only half filled, which causes the asymmetric distribution of the magnetomotive force (mmf) on the primary. The secondary of the discussed LSRM has a multipole structure and is composed of magnetically salient segments (Hamler *et al.*, 1998). The length of the segment is equal to the primary pole pitch. By putting segments together, any length of the secondary can be obtained. Each segment consists of semicircular lamellas cut out from electrical steel sheet. A filling is used to make the segment compact. The secondary segment shape is presented in Figure 1.

The magnetic conditions in the LSRM were computed by 2D FE method using the basic equation:

$$\mathrm{rot}\,(\nu\,\mathrm{rot}(A)) = J \tag{5}$$

where ν denotes the reluctivity, A is the magnetic vector potential and J is the current density. The LSRM thrust was calculated by the Maxwell's stress

tensor method using the integration path in the middle of the air-gap. The shape of the primary and secondary, and magnetic field distribution are presented in Figure 2. Because of the magnetic asymmetry (asymmetric mmf on the primary), the total length of the primary is included in the magnetic field calculation. The end winding leakage effects are not considered in the 2D FE calculations. These effects could be considered in the 3D FE models, which are in the case of tested LSRM too huge and too time-consuming to be used. The 3D FE calculations have not been performed because the 3D FE packages, which are able to handle 3D FE models of the LSRM in the size of a few 1,00,000 elements and to perform 2,592 calculations (36 combinations of currents i_d and i_q in 72 different positions) in acceptable time, are not available to the authors. The 2D FE model of the LSRM for the entire length of the primary contains more than 20,000 elements.

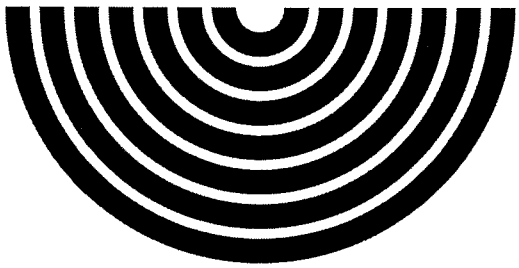

Figure 1.
Shape of secondary segments

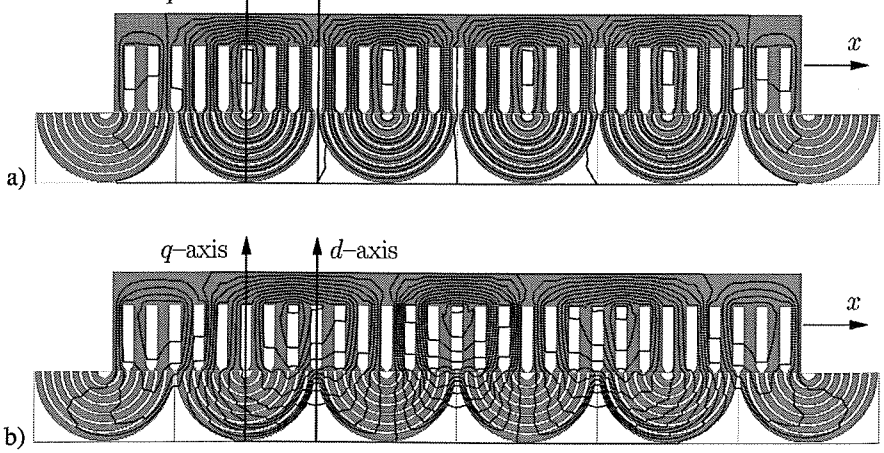

Figure 2.
Magnetic field distribution.
(a) Excitation in d-axis $i_d = 40$ A, $i_q = 0$ A;
(b) excitation in q-axis $i_d = 0$ A, $i_q = 40$ A (the direct axis is collinear with the magnetic axis of the a phase winding)

Indeed, the results obtained by the 2D FE computations might be less accurate than the ones obtained by the 3D FE computations, but they are still relevant enough to substantially improve dynamic behavior of the two-axis LSRM model.

The 2D FE method based procedure for the determination of current and position dependent flux linkages $\psi_d(i_d, i_q, x)$, $\psi_q(i_d, i_q, x)$ and thrust $F(i_d, i_q, x)$ of the two-axis dynamic LSRM model is described in the following steps.

Step 1. The FE model of the LSRM cannot be directly supplied by the instantaneous values of currents i_d and i_q, which are state variables of the two-axis dynamic LSRM model. Therefore, for the given position x and model currents i_d and i_q the instantaneous values of the phase currents i_a, i_b and i_c required in the FE model are calculated by:

$$\begin{bmatrix} i_a \\ i_b \\ i_c \end{bmatrix} = \sqrt{\frac{2}{3}} \begin{bmatrix} \cos(\Theta) & -\sin(\Theta) & \frac{\sqrt{2}}{2} \\ \cos\left(\Theta + \frac{4\pi}{3}\right) & -\sin\left(\Theta + \frac{4\pi}{3}\right) & \frac{\sqrt{2}}{2} \\ \cos\left(\Theta + \frac{2\pi}{3}\right) & -\sin\left(\Theta + \frac{2\pi}{3}\right) & \frac{\sqrt{2}}{2} \end{bmatrix} \begin{bmatrix} i_d \\ i_q \\ i_0 \end{bmatrix} \tag{6}$$

where $\Theta = (\pi/\tau_p)x$ and i_0 equals zero due to the Y connection.

Step 2. For the given position and phase currents, equation (5) is solved numerically.

Step 3. The thrust is calculated by the Maxwell's stress tensor method. The phase flux linkages are calculated from the average value of the magnetic vector potential in the primary slots according to the winding arrangement.

Step 4. The model flux linkages $\psi_d(i_d, i_q, x)$ and $\psi_q(i_d, i_q, x)$ are calculated from the phase flux linkages applying the inverse transformation used in equation (6).

Step 5. The procedure proceeds with Step 1 for a new set of x, i_d and i_q until calculations are performed in the entire operating range.

Both flux linkages, $\psi_d(i_d, i_q, x)$ and $\psi_q(i_d, i_q, x)$, are averaged over two pole pitches because they change just slightly with position at constant i_d and i_q. The averaged flux linkages $\psi_d(i_d, i_q)$, $\psi_q(i_d, i_q)$ and the current and position dependent thrust $F(i_d, i_q, x)$ are approximated by the continuous functions in the entire operating range and then incorporated into the dynamic LSRM model. The flux linkages are approximated by equation (7) and the thrust by equation (8):

$$\begin{aligned} f(u, v) = {} & (C_1 e^{-A_1 v} + C_2 e^{-A_2 v}) e^{-(C_3 e^{-A_3 v} + C_4 e^{-A_4 v})u} \\ & + (C_5 e^{-A_5 v} + C_6 e^{-A_6 v}) e^{-(C_7 e^{-A_7 v} + C_8 e^{-A_8 v})u} \end{aligned} \tag{7}$$

$$F(i_d, i_q, x) = f_0(i_d, i_q) + f_1(i_d, i_q)\sin(Bx) + f_2(i_d, i_q)\sin\left(\frac{12\pi}{\tau_p}x\right) + f_3(i_d, i_q)\sin\left(\frac{24\pi}{\tau_p}x\right) \quad (8)$$

where $\psi_d(i_d, i_q)$, $\psi_q(i_d, i_q)$ and $f_0(i_d, i_q)$ through $f_3(i_d, i_q)$ have the same structure as $f(u, v)$ (equation (7)). The parameters C_1 through C_8, A_1 through A_8 and B were determined by the Nelder-Mead simplex direct search method (Nelder and Mead, 1965) and the differential evolution (Storn and Price, 1996).

4. Results

The comparison of the measured LSRM thrust and that derived from the Maxwell's stress tensor method is given in Figure 3 over one pole pitch for different constant currents i_d and i_q. The agreement between the measured and the calculated results is very good.

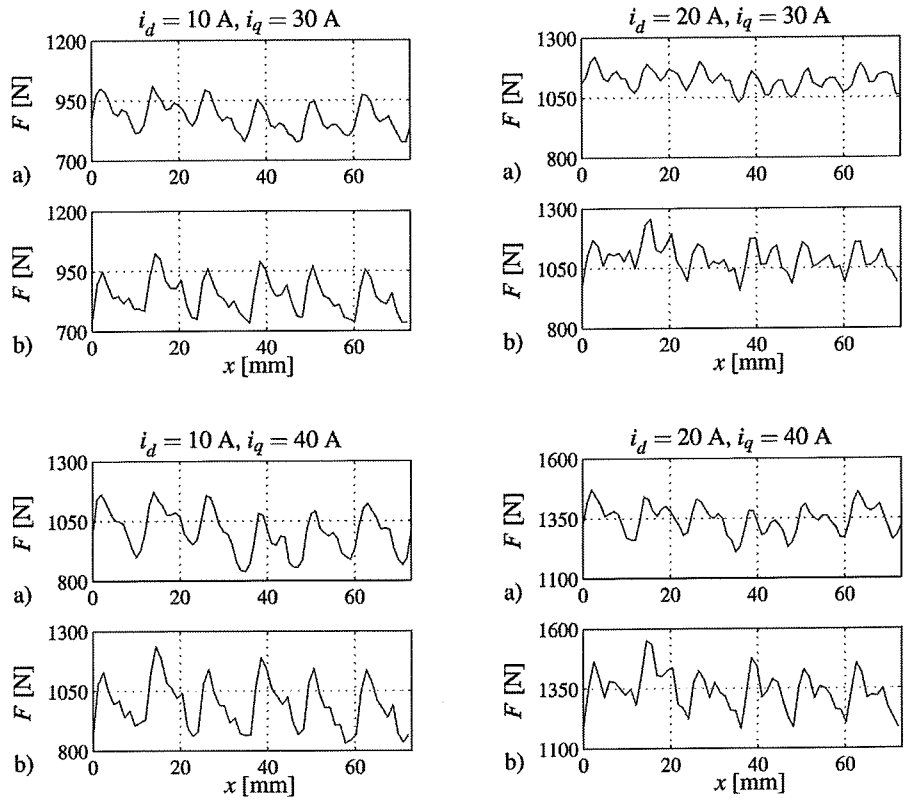

Figure 3.
LSRM thrusts given over one pole pitch.
(a) Measured;
(b) calculated by the Maxwell's stress tensor method

A comparison of the measured, FE method calculated and continuous functions approximated flux linkages and their partial derivatives is given in Figures 4-6. The partial derivatives of the measured and FE calculated flux linkages are approximated by differential quotients (9) for each set of i_d and i_q, while the partial derivatives of the continuous functions are determined analytically.

$$\frac{\partial \psi_d}{\partial i_d} \approx \frac{\Delta \psi_d}{\Delta i_d} \quad \frac{\partial \psi_d}{\partial i_q} \approx \frac{\Delta \psi_d}{\Delta i_q} \quad \frac{\partial \psi_q}{\partial i_d} \approx \frac{\Delta \psi_q}{\Delta i_d} \quad \frac{\partial \psi_q}{\partial i_q} \approx \frac{\Delta \psi_q}{\Delta i_q} \tag{9}$$

The agreement among measured, calculated and continuous functions approximated flux linkages and their partial derivatives is very good. The partial derivatives are close to satisfying the condition for the conservative system without any loss of energy in the iron core: $\partial \psi_q / \partial i_d = \partial \psi_d / \partial i_q$ (Sauer, 1992).

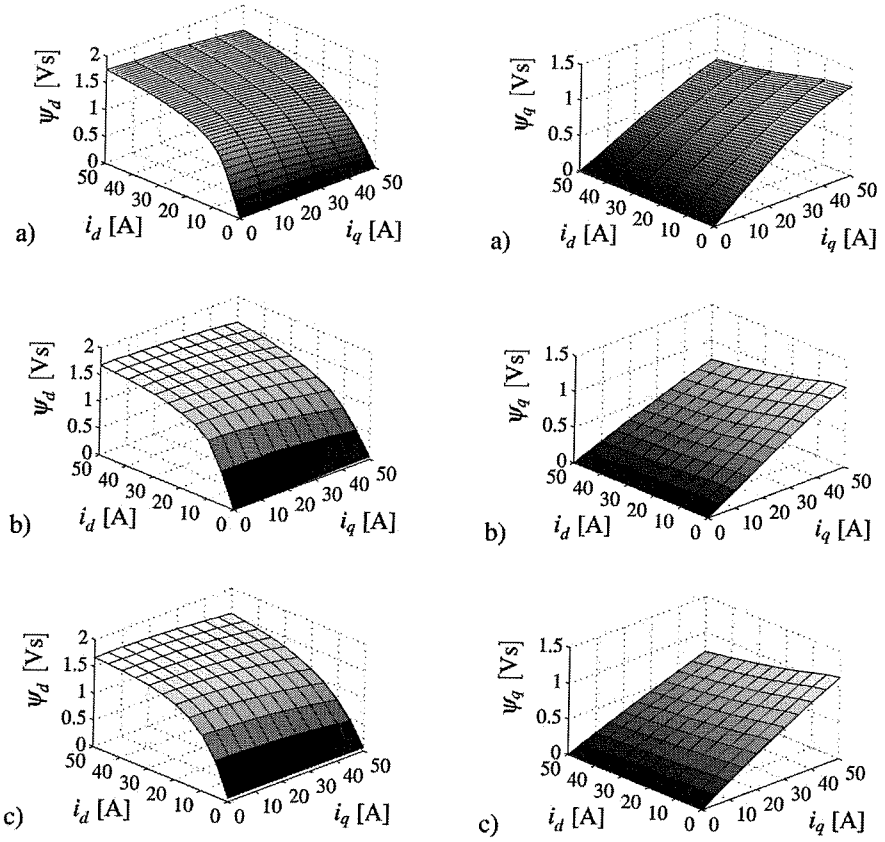

Figure 4.
Flux linkages ψ_d and ψ_q. (a) Measured; (b) calculated by the FE method; and (c) approximated by continuous functions

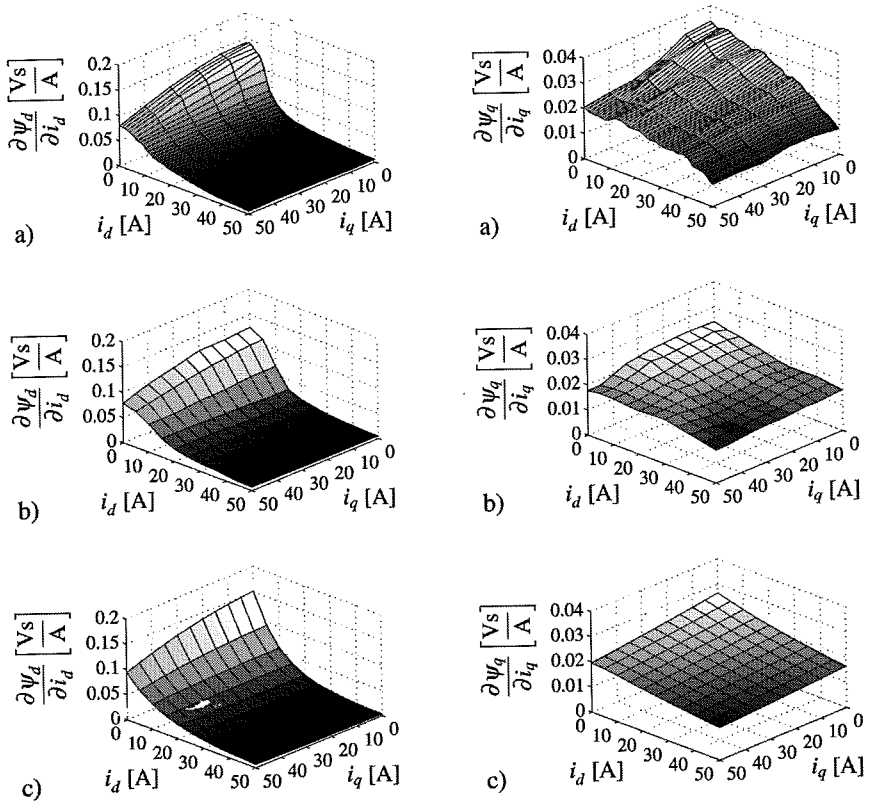

Figure 5.
Partial derivatives $\partial\psi_d/\partial i_d$ and $\partial\psi_q/\partial i_q$.
(a) Measured;
(b) calculated by the FE method; and
(c) approximated by continuous functions

FE calculated and continuous functions approximated flux linkages ($\psi_d(i_d, i_q)$ and $\psi_q(i_d, i_q)$) and LSRM thrust $F(i_d, i_q, x)$ were incorporated into the dynamic LSRM model. Figure 7 gives the comparison of trajectories measured during the experiment and calculated by the proposed dynamic LSRM model in the case of kinematic control. The agreement of all trajectories is very good. The influence of the position dependent thrust pulsation on the trajectories of speed v and current i_q, characteristic for the low speed servo application, is clearly seen in both the measured and simulated results.

During the experiment, the tested LSRM was supplied by a controlled voltage source inverter, while in the simulation its model was given by a static element with the unity gain. All the nonlinear and dynamic properties of the inverter, including properties of the pulse width modulation, were neglected. The trajectories of the reference voltages u_d and u_q recorded during the experiment differ slightly from the calculated ones due to the simplified model of the voltage source inverter. The difference between the recorded and calculated trajectories of the reference voltage u_d can be seen in Figure 7.

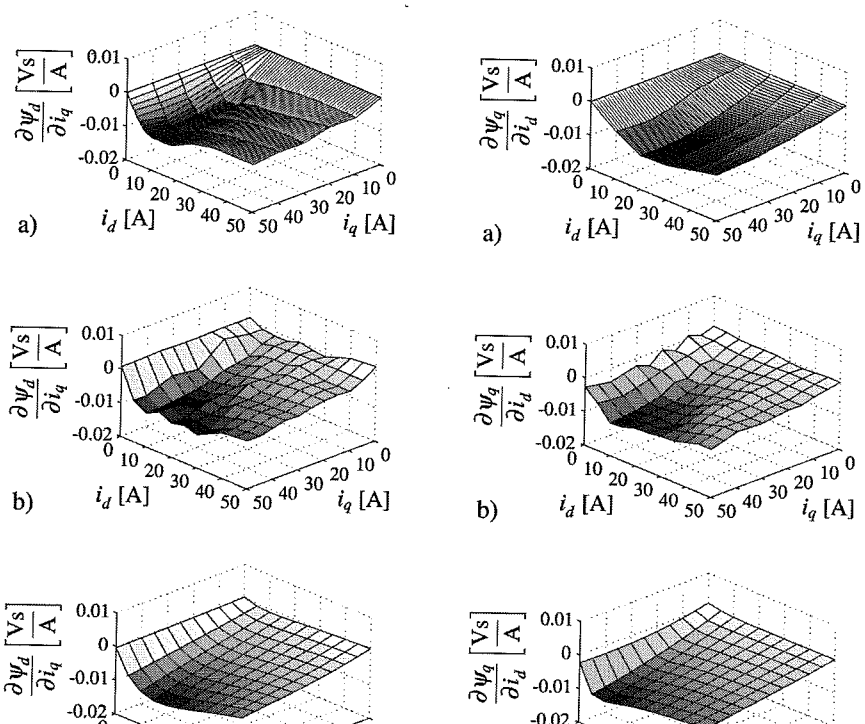

Figure 6.
Partial derivatives $\partial\psi_d/\partial i_q$ and $\partial\psi_q/\partial i_d$.
(a) Measured;
(b) calculated by the FE method; and
(c) approximated by continuous functions

The currents i_d and i_q were close loop controlled, therefore the agreement between their measured and calculated trajectories is very good.

5. Conclusion

The FE method based procedure for the calculation of current and position dependent LSRM thrust and flux linkages is presented in the paper. The two-axis dynamic LSRM model with lumped parameters is modified and improved by incorporating the results of the FE calculations. The improved LSRM model contains appropriately coupled models of the electric, magnetic and mechanical subsystem. It is suitable for the control design, real time applications, and low speed servo applications. The proposed model is confirmed through the comparison of trajectories obtained by the experiment and by the simulation in the case of kinematic control. The agreement of presented results is very well achieved by combining the dynamic model with results of the FE.

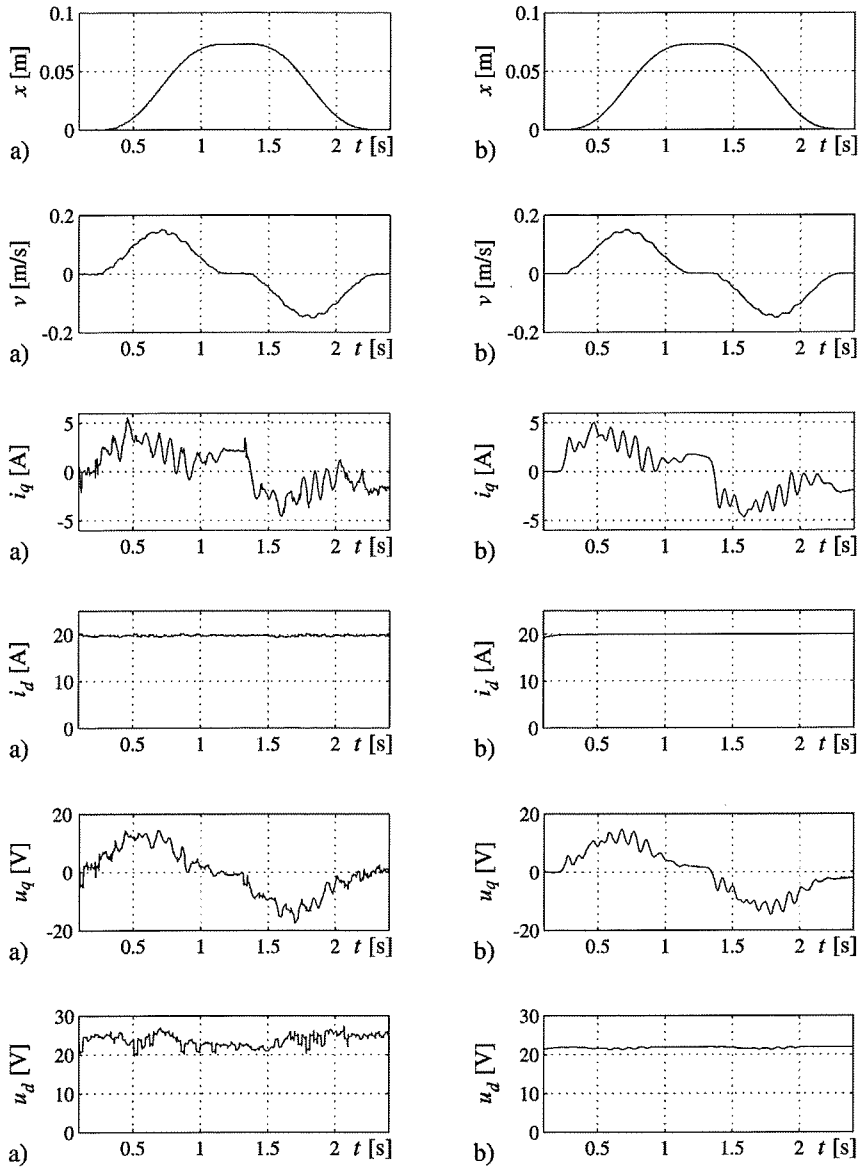

Figure 7.
Trajectories of position x, speed v, currents i_d, i_q and voltages u_d, u_q in the case of kinematic control. (a) Experiment; and (b) simulation

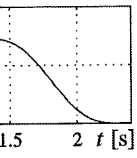

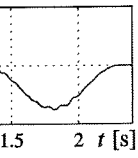

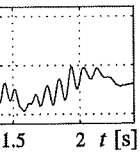

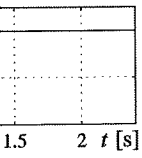

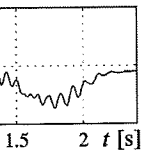

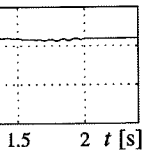

References

Boldea, I. and Nasar, S.A. (1988), "A general equivalent circuit (GEC) of electric machines including crosscoupling saturation and frequency effects", *IEEE Trans. on Energy Conversion*, Vol. 3 No. 3, pp. 689-95.

Dawson, D., Hu, J. and Burg, T. (1998), *Nonlinear Control of Electric Machinery*, Marcel Dekker, Inc., New York.

Hamler, A., Trlep, M. and Hribernik, B. (1998), "Optimal secondary segment shape of linear reluctance motor using stochastic searching", *IEEE Trans. on Magn.*, Vol. 34 No. 5, pp. 3519-21.

Ho, S., Li, H., Fu, W. and Wong, H. (2000), "A novel approach to circuit-torque coupled time stepping finite element modeling of electric machines", *IEEE Trans. on Magn.*, Vol. 36 No. 4, pp. 1886-9.

Iglesias, I., Garcia-Tabares, L. and Tamarit, J. (1992), "A d-q model for the self-commutated synchronous machine considering the effects of magnetic saturation", *IEEE Trans. on Energy Conversion*, Vol. 7 No. 4, pp. 768-76.

Kim, J.C., Lee, J.H., Jung, I.S. and Hyun, D.S. (1998), "Vector control scheme of synchronous reluctance motor considering iron core loss", *IEEE Trans. on Magn.*, Vol. 34 No. 5, pp. 3522-5.

Levi, E. (1999), "Saturation modelling in d-q axis models of salient pole synchronous machines", *IEEE Trans. on Energy Conversion*, Vol. 14 No. 1, pp. 44-50.

Nelder, J. and Mead, R. (1965), "A simplex method for function minimization", *Computer Journal*, No. 7, pp. 308-13.

Ren, Z. and Razek, A. (1994), "A strong coupled model for analysing dynamic behaviours of non-linear electromechanical systems", *IEEE Trans. on Magn.*, Vol. 30 No. 5, pp. 3252-5.

Sauer, P.W. (1992), "Constraints on saturation modeling in AC machines", *IEEE Trans. on Energy Conversion*, Vol. 7 No. 1, pp. 161-7.

Srairi, K. and Féliachi, M. (1998), "Numerical coupling models for analyzing dynamic behaviors of electromagnetic actuators", *IEEE Trans. on Magn.*, Vol. 34 No. 5, pp. 3608-11.

Storn, R. and Price, K. (1996), "Minimizing the real functions of the ICEC'96 contest by differential evolution", *IEEE Conference on Evolutionary Computation*, IEEE, Nagoya, Japan, pp. 842-4.

Tahan, S.A. and Kamwa, I. (1995), "A two-factor saturation model for synchronous machines with multiple rotor circuits", *IEEE Trans. on Energy Conversion*, Vol. 10 No. 4, pp. 609-16.

Xu, L., Xu, X., Lipo, T.A. and Novotny, D.W. (1991), "Vector control of a synchronous reluctance motor including saturation and iron loss", *IEEE Trans. on Ind. Appl.*, Vol. 27 No. 5, pp. 977-85.